Acta Mech 230, 953–964 (2019)
https://doi.org/10.1007/s00707-018-2276-2

ORIGINAL PAPER

Rui Li · Dianyun Zhang

A textile architecture-based hyperelastic model for rubbers reinforced by knitted fabrics

Received: 11 May 2018 / Revised: 8 August 2018 / Published online: 13 December 2018

Abstract A new anisotropic hyperelastic model has been developed to model the deformation response of a knitted-fabric-reinforced rubber composite. The composite has a sandwich structure with a fiber net layer embedded in two rubber layers. Due to the architecture of the knitted fabric, the composite demonstrates an anisotropic hyperelastic response, which is modeled through a strain energy density function that incorporates the effects of deformed rubbers and stretched fibers. The rubber is considered as a neo-Hookean material, while the knitted fabrics are modeled as cords with negligible stiffness in bending. The effect of reinforcement comes from the conservation of the total length of the fiber cords. In addition, a slack variable is proposed to account for the effect of processing-induced fabric pre-stretch or fabric slack on the resulting composite response. This novel approach enables the determination of the constitutive behavior of the composite in closed form based on the constituent rubber and fiber properties and fabric architectures. The proposed analytical model is validated through a full 3D finite element (FE) model, in which the rubber and fiber reinforcement are modeled explicitly. Since the proposed model captures the key parameters that dictate the deformation response of knitted-fabric-reinforced composites, it can be employed as an efficient modeling tool to guide the design of rubbers and fabric architectures with targeted composite performance.

1 Introduction

Fiber-reinforced rubber hoses are widely used in many industrial areas for liquid and gas transportation. Advances in textile technologies including stitching, weaving, braiding, and knitting allow for various fabric architectures to be used as reinforcements. It has been found that the deformation response of a composite hose is significantly affected by the textile pattern [1]. Specifically, a knitted-fabric-reinforced rubber composite shows a lower longitudinal modulus than that of other types of fabric reinforcements [2]. The low resistance to deformation makes the knitted-fabric-reinforced composite a good candidate for hoses of complex geometry, such as coolant hoses used in engine systems.

However, the anisotropic nature of these composites makes their characterization a great challenge. To fully characterize the mechanical properties, dumbbell specimens should be prepared for simple tensile tests according to ASTM D412 [3]. It is also worth mentioning that these fiber-reinforced rubber composites are usually manufactured into hoses through an extruding process. As a result, it is inevitable to cut the fabric reinforcements when preparing the testing samples. However, due to the fact that the modulus of the fiber is much higher than that of the rubber, the fabric reinforcements tend to slip into the rubber layers when the composite is under external loading, resulting in an inaccurate measurement of the hose properties. If mechanical tests are performed directly on the composite hose, only axial tension and axial shear responses can

R. Li · D. Zhang (✉)
Department of Mechanical Engineering, University of Connecticut, 191 Auditorium Road, Unit 3139, Storrs, CT 06269-3139, USA
E-mail: dianyun.zhang@uconn.edu

be obtained according to ASTM D380 [4] and E143 [5], respectively. Therefore, a physics-based constitutive model based on the rubber and fabric properties should be developed in conjunction with limited experimental data of the hose to fully understand the deformation response of rubber composites.

The challenge of modeling these rubber composites lies in the hyperelastic response of the rubber combined with the geometric nonlinearity resulting from fiber deformation [6]. The finite element (FE) method has been widely adopted to predict the mechanical response of the composite by explicitly modeling the rubber and fabric microstructure [7–10]. However, this method requires high computational costs, making it impossible for large-scale structural analysis. In addition, additional experiments are required to characterize the interaction between the fabric and the rubber.

As such, many studies are focused on the development of homogenization techniques for rubber composites. These models usually treat the composite as an orthotropic solid, and the effective properties are determined based on the constituent rubber and reinforcement properties through micromechanics [11–14]. However, critical information such as the rubber's nonlinear behavior, architecture of the reinforced cords, and rotation of the cords during deformation are ignored in these orthotropic elastic models, limiting their applications for analysis involving large deformation.

To account for the hyperelastic response of the rubber, many researchers have developed nonlinear constitutive models based on strain energy functions [15–20]. The main idea to incorporate the fiber reinforcement is to decompose the strain energy function into two parts, including the strain energy due to the rubber deformation and the strain energy stored in the stretched fibers. The normal and shear interactions between the fiber and rubber can also be incorporated into the strain energy functions [21–23]. The effect of fabric architecture is captured by introducing an orientation vector which dictates the stretch of each fiber family [20,24,25]. However, little research has been done to investigate the reinforcement effect of knitted fabrics in rubber composites.

The objective of this study is to develop a constitutive model for knitted-fabric-reinforced rubber composites through a strain energy density function that incorporates the hyperelastic response of the rubber and the reinforcement effect of the knitted fibers. The paper is organized as follows. Section 2 shows the development of a new strain energy function for knitted-fiber-reinforced composites along with the approach to determine material constitutive models based on strain energy functions. The effect of processing on the resulting composite response is also considered. The proposed analytical model is further validated through a discrete 3D FE model, as discussed in Sect. 3. The deformation response of the rubber composite, the effect of knitted fabric pattern and processing-induced variations are presented in Sect. 4.

2 Development of the strain energy density function for a knitted-fabric-reinforced rubber composite

2.1 Preliminaries

Consider a soft composite consisting of rubber layers and knitted fabrics, as shown in Fig. 1. Such a composite can be homogenized as an anisotropic hyperelastic solid, whose deformation response can be dictated through an appropriate strain energy density function, $W = W(\boldsymbol{F})$, which depends only on the material properties and the deformation state. The deformation gradient tensor is expressed as $\boldsymbol{F} = \dfrac{\partial \boldsymbol{x}}{\partial \boldsymbol{X}}$, where $\boldsymbol{X}$ denotes the position in the reference configuration, and $\boldsymbol{x}$ denotes the position in the deformed configuration. To satisfy the principle of objectivity, the strain energy density function is rewritten in terms of the right Cauchy deformation tensor, $\boldsymbol{C} = \boldsymbol{F}^{\mathrm{T}}\boldsymbol{F}$, as

$$W = W(\boldsymbol{C}). \tag{1}$$

Thus, the second Piola–Kirchhoff (PK) stress $\boldsymbol{S}$ can be calculated directly from the strain energy density function in terms of the right Cauchy–Green deformation tensor as

$$\boldsymbol{S} = 2\frac{\partial W(\boldsymbol{C})}{\partial \boldsymbol{C}}. \tag{2}$$

To consider the effect of fiber reinforcement, let the unit vector $\boldsymbol{A}_s^{(k)}$ denote the orientation of the kth fiber segment with an initial length $L_s^{(k)}$.

Moreover, we define the first invariant I_1 and the pseudo-invariants $I_{4s}^{(k)}$ of the right Cauchy–Green deformation tensor as

$$I_1 = \mathrm{tr}(\boldsymbol{C}), \tag{3}$$

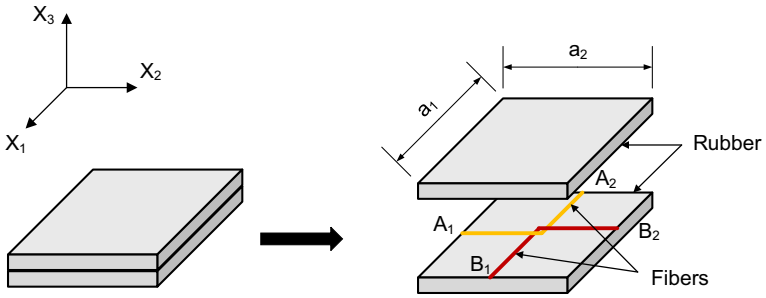

Fig. 1 Illustration of a knitted-fabric-reinforced rubber composite

$$I_{4s}^{(k)} = (\boldsymbol{A}_s^{(k)})^{\mathrm{T}} \boldsymbol{C} (\boldsymbol{A}_s^{(k)}). \tag{4}$$

In addition, the isochoric part of the right Cauchy–Green deformation tensor, $\bar{\boldsymbol{C}}$, is related to $\boldsymbol{C}$ as

$$\bar{\boldsymbol{C}} = [\det(\boldsymbol{C})]^{-\frac{1}{3}} \boldsymbol{C} = J^{-\frac{2}{3}} \boldsymbol{C}, \tag{5}$$

where J is the local ratio of volume change given by $J = \det(\boldsymbol{F})$. $\bar{I}_1$ is defined as the first invariant of $\bar{\boldsymbol{C}}$ [24].

2.2 Development of the strain energy density function

In this section, we provide a strain energy density function to dictate the deformation response of a rubber-like material reinforced by knitted fabrics. The rubber composite is shown in Fig. 1, where the fiber reinforcement is embedded in two rubber layers. Since the hyperelastic response of a pure rubber can be modeled as a neo-Hookean solid, the goal is to incorporate the reinforcement effect of the knitted fabrics in the strain energy density function. To use the invariant formulation for the fiber-reinforced rubber, the stored energy density per unit undeformed volume can be expressed as

$$W = W\left(I_1, J, I_{4s}^{(k)}\right). \tag{6}$$

In this study, we ignore the friction between fiber and rubber. Thus, the strain energy density function of the composite consists of the strain energy density of the rubber deformation (W_{r}) and the fiber stretch (W_{f}) as

$$W = (1 - V_{\mathrm{f}}) W_{\mathrm{r}} + V_{\mathrm{f}} W_{\mathrm{f}}, \tag{7}$$

where V_{f} is the fiber volume fraction. Here, the neo-Hookean model is employed to dictate the hyperelastic response of the rubber as

$$W_{\mathrm{r}} = \frac{\mu}{2}(\bar{I}_1 - 3) + \frac{K}{2}(J - 1)^2, \tag{8}$$

where μ and K are the initial shear and bulk modulus of the rubber.

The strain energy density of the fiber, W_{f}, which is determined based on the deformation of the fibers, should capture the textile architecture of the reinforcing fabric. For knitted fabrics, as schematically shown in Fig. 2, the bending stiffness is negligible. Thus, we assume that only the *stretch* of the fiber will contribute to the strain energy. Note that the knitted fiber net has a repeating pattern (see Fig. 2b), which can be represented by two different reinforcing architectures as shown in Fig. 2c. In each architecture, there are two loops of fibers to secure a stitch, and the strain energy due to fiber stretch is the same. Thus, a Representative Unit Cell (RUC) shown in Fig. 1 can be employed to further determine the strain energy of the rubber composite. In the RUC, a representative fiber layer is embedded at the middle of two rubber layers. The stretch of the fiber segments, λ_{f}, in the RUC becomes

$$\lambda_{\mathrm{f}} = \frac{l}{L}, \tag{9}$$

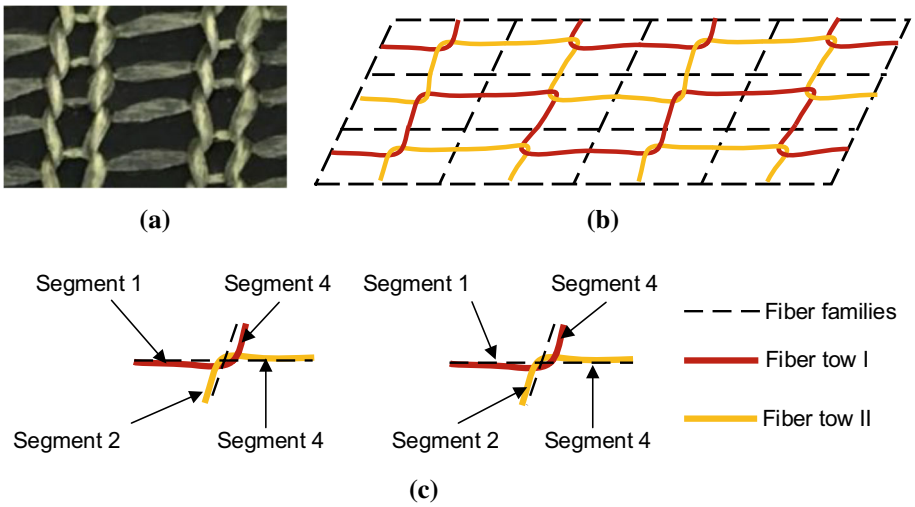

Fig. 2 Representation of the knitted fiber net. **a** Image of the fiber net. **b** Schematic of the fiber net. **c** Fiber pattern in the RUC

where L and l are the total length of the fibers in the RUC in the undeformed and deformed state, respectively. It should be noted that λ_f is the overall stretch ratio of all the fibers in the RUC. For m segments of fibers, L and l become

$$L = \sum_{k=1}^{m} L_s^{(k)}, \tag{10}$$

$$l = \sum_{k=1}^{m} l_s^{(k)}. \tag{11}$$

The length $l_s^{(k)}$ of the kth fiber segment in the deformed configuration can be expressed in terms of the initial length $L_s^{(k)}$ of the kth fiber segment in the reference configuration, the orientation vector $\boldsymbol{A}^k$, and the deformation state as

$$l_s^{(k)} = \sqrt{\left(L_s^{(k)} \boldsymbol{F} \boldsymbol{A}^{(k)}\right) \cdot \left(L_s^{(k)} \boldsymbol{F} \boldsymbol{A}^{(k)}\right)} = L_s^{(k)} \sqrt{\left(\boldsymbol{A}^{(k)}\right)^{\mathrm{T}} \boldsymbol{C} \boldsymbol{A}^{(k)}} = L_s^{(k)} \sqrt{I_{4s}^{(k)}}. \tag{12}$$

Then, the stretch of the fiber segments in the RUC becomes

$$\lambda_f = \frac{\sum_{k=1}^{m} L_s^{(k)} \sqrt{I_{4s}^{(k)}}}{\sum_{k=1}^{m} L_s^{(k)}}. \tag{13}$$

2.3 Effects of manufacturing processes on the resulting response

Due to the manufacturing process, initial stresses can be developed in the fiber tows and rubber during curing. It is assumed that at the curing temperature, the rubber experiences shrinkage while the fiber is not affected by the temperature. The rubber shrinkage during the curing process gives rise to a compressive force applied on the fiber tows. However, the fiber tows cannot carry compressive load which results in fiber slacking. To straighten the fiber tows in the composite, the fiber tows can be pre-stretched during the manufacturing process. In this study, both rubber shrinkage and fabric pre-stretch are considered through the incorporation of a slack variable. The slack variable represents the initial stress state of the fiber tows caused by the rubber curing shrinkage or the pre-stretch of the fiber tows. A slack variable that is greater than 1.0 indicates that the fiber tows are in the loose state caused by the rubber curing shrinkage. The slack variable is smaller than 1.0 when

the fiber tows are pre-stretched. Thus, the strain energy density of the fiber segments in the RUC can be written in terms of the fiber modulus (E_f), volume fraction (V_f), stretch ratio (λ_f), and slack variable (s) as

$$V_\mathrm{f} W_\mathrm{f} = \frac{E_\mathrm{f} V_\mathrm{f}}{2}(\lambda_\mathrm{f} - s)^2 = \frac{E_\mathrm{f} V_\mathrm{f}}{2}\left(\frac{\sum_{k=1}^{m} L_s^{(k)}\sqrt{I_{4s}^{(k)}}}{\sum_{k=1}^{m} L_s^{(k)}} - s\right)^2. \tag{14}$$

Finally, the strain energy function for the knitted-fabric-reinforced rubber composite becomes

$$W = (1 - V_\mathrm{f})\left(\frac{\mu}{2}(\bar{I}_1 - 3) + \frac{K}{2}(J-1)^2\right) + \frac{E_\mathrm{f} V_\mathrm{f}}{2}\left(\frac{\sum_{k=1}^{m} L_s^{(k)}\sqrt{I_{4s}^{(k)}}}{\sum_{k=1}^{m} L_s^{(k)}} - s\right)^2, \tag{15}$$

where the first two terms dictate the strain energy of the rubber, and the last term dictates the strain energy due to fiber stretch.

The second Piola–Kirchhoff (P–K) stress tensor is computed through the chain rule as

$$\boldsymbol{S} = 2\frac{\partial W}{\partial \bar{I}_1}\frac{\partial \bar{I}_1}{\partial \boldsymbol{C}} + 2\frac{\partial W}{\partial J}\frac{\partial J}{\partial \boldsymbol{C}} + 2\sum_{k=1}^{m}\left(\frac{\partial W}{\partial I_{4s}^{(k)}}\frac{\partial I_{4s}^{(k)}}{\partial \boldsymbol{C}}\right). \tag{16}$$

After some straightforward manipulations, the third term in Eq. (16) can be written as

$$2\sum_{k=1}^{m}\left(\frac{\partial W}{\partial I_4^{(k)}}\frac{\partial I_4^{(k)}}{\partial \boldsymbol{C}}\right) = \frac{E_\mathrm{f} V_\mathrm{f}}{L}\left(\frac{l}{L} - s\right)\sum_{k=1}^{m}\left(\frac{L_s^{(k)}}{\sqrt{I_{4s}^{(k)}}}\boldsymbol{A}^{(k)} \otimes \boldsymbol{A}^{(k)}\right). \tag{17}$$

Consider the relation between the Cauchy stress and the second P–K stress,

$$J\boldsymbol{\sigma} = \boldsymbol{F}\boldsymbol{S}\boldsymbol{F}^\mathrm{T}. \tag{18}$$

The Cauchy stress can be written as

$$\boldsymbol{\sigma} = (1 - V_\mathrm{f})\left(J^{-1}\mu\left(\bar{\boldsymbol{B}} - \frac{\bar{I}_1}{3}\boldsymbol{I}\right) + K(J-1)\boldsymbol{I}\right) + \frac{E_\mathrm{f} V_\mathrm{f}}{JL}\left(\frac{l}{L} - s\right)\boldsymbol{F}\sum_{k=1}^{m}\left(\frac{L_s^{(k)}}{\sqrt{I_{4s}^{(k)}}}\boldsymbol{A}^{(k)} \otimes \boldsymbol{A}^{(k)}\right)\boldsymbol{F}^\mathrm{T}, \tag{19}$$

where $\bar{\boldsymbol{B}} = J^{(-2/3)}\boldsymbol{B}$ is the isochoric part of the Left Cauchy–Green deformation tensor $\boldsymbol{B} = \boldsymbol{F}\boldsymbol{F}^\mathrm{T}$.

The Cauchy stress shown in Eq. (19) indicates that deformation response of the knitted-fabric-reinforced rubber composite is determined based on the fabric architecture including the initial length and the orientation. This also suggests that the two architectures shown in Fig. 2c should give the same results since the four fiber segments are of the same total length and orthogonally interlocked. In this paper, the fiber segments in the same direction are defined as one fiber family shown in Fig. 2c. Based on the Eq. (19), the Cauchy stress is computed based on the length of each fiber family, and Eq. (19) can be rewritten as

$$\boldsymbol{\sigma} = (1 - V_\mathrm{f})\left(J^{-1}\mu\left(\bar{\boldsymbol{B}} - \frac{\bar{I}_1}{3}\boldsymbol{I}\right) + K(J-1)\boldsymbol{I}\right) + \frac{E_\mathrm{f} V_\mathrm{f}}{JL}\left(\frac{l}{L} - s\right)\boldsymbol{F}\sum_{k=1}^{n}\left(\frac{L_\mathrm{f}^{(k)}}{\sqrt{I_{4\mathrm{f}}^{(k)}}}\boldsymbol{A}_\mathrm{f}^{(k)} \otimes \boldsymbol{A}_\mathrm{f}^{(k)}\right)\boldsymbol{F}^\mathrm{T} \tag{20}$$

where n is the number of fiber families, $L_\mathrm{f}^{(k)}$ is the total length of the fiber segments belonging to the kth fiber family with orientation $\boldsymbol{A}_\mathrm{f}^{(k)}$, and $I_{4\mathrm{f}}^{(k)} = (\boldsymbol{A}_\mathrm{f}^{(k)})^\mathrm{T}\boldsymbol{C}(\boldsymbol{A}_\mathrm{f}^{(k)})$.

3 Validation of the strain energy function approach using FE analysis

To validate the proposed strain energy function of the knitted-fabric-reinforced rubber composite, a discrete 3D FE model is developed to model the composite explicitly. The FE analysis was conducted using the commercial FE software Abaqus (version 6.14-2). To save computational cost, the composite is represented by the RUC shown in Fig. 1. Uniaxial tension, biaxial tension, shear, and a general stress state including both normal and shear stresses are used as the representative cases to compare the stress–stretch relation computed using the FE model and the analytical approach. The effect of knitting fiber architecture on the resulting deformation response is given in Sect. 4.

3.1 Construction of the FE model

The geometry of the RUC for the discrete model used in this study is illustrated in Fig. 3. The two fiber tows, A_1–O–A_2 and B_1–O–B_2, are orthogonally interlocked at Point O. The rubber is modeled as a hyperelastic solid cuboid using the C3D8H elements. The volume of the reinforcing fibers, which is approximately 2% of the entire composite, can be neglected in the FE model. The reinforcement effect is realized by modeling the embedded fibers using the SLIPRING connector elements available in Abaqus. The SLIPRING connector element is used to model the material flow and stretch between two nodes of a belt system with negligible roller radius, such as a and b shown in Fig. 4. In the FE model, the fiber tow A_1–O–A_2 is modeled by 3 points A_1, O_1 and A_2 connected by two SLIPRING connectors A_1–O_1 and O_1–A_2. Similarly, the fiber B_1–O–B_2 is modeled by 3 points B_1, O_2 and B_2 connected by two SLIPRING connectors B_1–O_2 and O_2–B_2. Two dummy nodes O_1 and O_2 are used for the two fiber tows at O. The degree of freedom of the two dummy nodes O_1 and O_2 are constrained by kinematic coupling to mimic the knitting effect at point O. To ensure continuity between the adjacent RUCs, periodic boundary conditions are imposed on pairs of opposite boundary surfaces shown in Fig. 3.

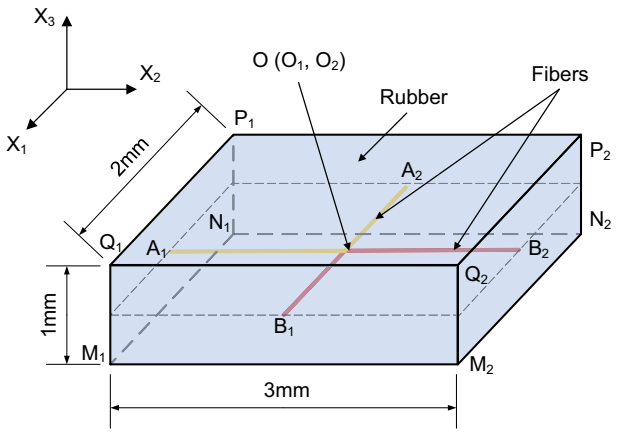

Fig. 3 3D FE model used in this study

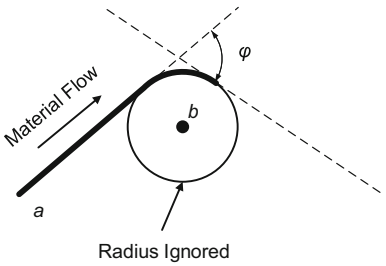

Fig. 4 The schematic of the SLIPRING connector in ABAQUS

3.2 Material properties

The hyperelastic response of the rubber is modeled using the neo-Hookean model available in the Abaqus material library through two input parameters, C_{10} and D_1. The relation between the material parameters in Abaqus and our proposed model is that $\mu = 2C_{10}$ and $K = \dfrac{2}{D_1}$. The SLIPRING connector is considered as a linear elastic material. The fiber elastic modulus along the longitudinal direction is specified for the SLIPRING element via the connector elasticity property through $D_{11} = AE_{\mathrm{f}}$, where D_{11} is the input parameter to dictate the stiffness of the connector, A is the cross-sectional area of the fiber tow, and E_{f} is the elastic modulus of the fiber. The fiber slacking is simulated by defining the reference length of the SLIPRING connector. In addition, the fiber volume fraction can be computed as $V_{\mathrm{f}} = AL_0/V_0$, where L_0 and V_0 are the total fiber length and volume, respectively, in the undeformed RUC. The material properties used in the FE model are summarized in Table 1.

3.3 Comparison between the FE model and the analytical approach

To thoroughly validate the proposed strain energy-based approach, the results computed from the discrete FE model are compared with those obtained from the proposed analytical model through a set of studies including uniaxial tension, biaxial tension, pure shear, and combined tension and shear loading conditions, as shown in Figs. 5, 6, 7, 8, respectively. The stretch ratio is computed through $\lambda = (L_0 + \Delta)/L_0$, where L_0 is the initial length of the RUC. The nominal stress in the FE model is computed through dividing the total reaction force by the initial area of the surface. The nominal stress in the analytical model is computed as $\boldsymbol{N} = J\boldsymbol{F}^{-1}\boldsymbol{\sigma}$. Since the fiber tows are modeled using the SLIPRING elements in Abaqus that ignore the volume of the fibers, it shows a slight deviation in the combined normal and shear loading condition when the deformation is large. Overall, it can be concluded that the results computed using the strain energy-based analytical model show good agreement with those based on the FE model. The proposed analytical model shows a significant computational advantage since the analysis is carried out in closed form. As such, it is further employed to study the effect of fabric architecture on the deformation response of the composite.

Table 1 The material properties used in the validation study

C_{10} (MPa)	D_1 (MPa)	D_{11} (MPa mm^2)
2.0	1×10^{-4}	2.4×10^3

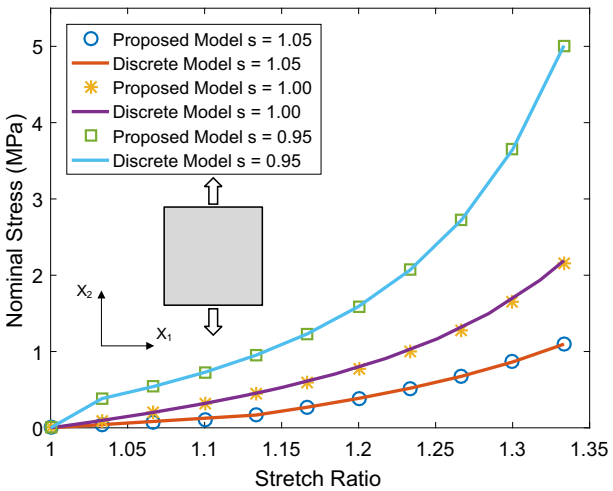

Fig. 5 Comparison of the uniaxial tension response obtained from the proposed model and the discrete FE model with various slack variables

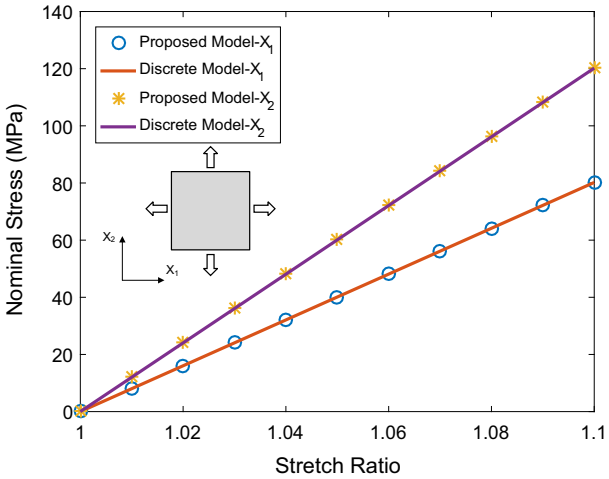

Fig. 6 Comparison of the biaxial tension response obtained from the proposed model and the discrete FE model

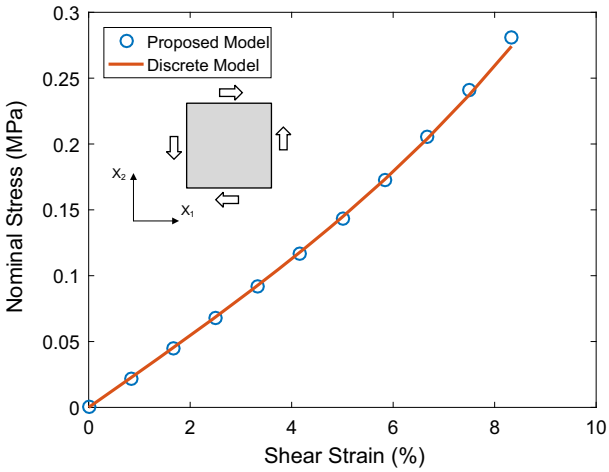

Fig. 7 Comparison of the pure shear response obtained from the proposed model and the discrete FE model

4 Effects of fabric architectures on the deformation response of the rubber composite

In this section, the proposed strain energy function is employed to study the effect of knitting fiber architecture on the resulting deformation response. In this paper, we focus on the knitted pattern with two fiber tows that are interlocked orthogonally as shown in Fig. 1. Note that these knitted-fabric-reinforced rubber composites are usually manufactured into hoses to transport liquid or gas, and the two orthogonal families of fibers are aligned with the axial and hoop directions of the hose. Then, the length ratio of the fibers in the two orthogonal directions, which can be characterized as the aspect ratio of the RUC shown in Fig. 1, determines how the composite is reinforced in the two directions. It is also worth mentioning that the proposed strain energy function can be applied to any general knitting patterns by modifying the orientation vector of each knitting fiber family. If the fibers are interlocked at an angle other than 90°, the overall composite response becomes non-orthotropic. That is, a uniaxial tensile loading can induce shear deformation and vice versa. A separate study on the effect of interlock angle and how the angle is induced during manufacturing is a subject of future investigation.

Let X_1, X_2, and X_3 denote the axes of the Cartesian coordinate system shown in Fig. 1. For an orthogonally interlocked fiber net, the local orientations of the two fiber families, $A_2 - O - B_1$ and $A_1 - O - B_2$, are

$$\boldsymbol{A}_{\mathrm{f}}^{(1)} = \begin{pmatrix} 1 \\ 0 \\ 0 \end{pmatrix} \quad \text{and} \quad \boldsymbol{A}_{\mathrm{f}}^{(2)} = \begin{pmatrix} 0 \\ 1 \\ 0 \end{pmatrix}. \tag{21}$$

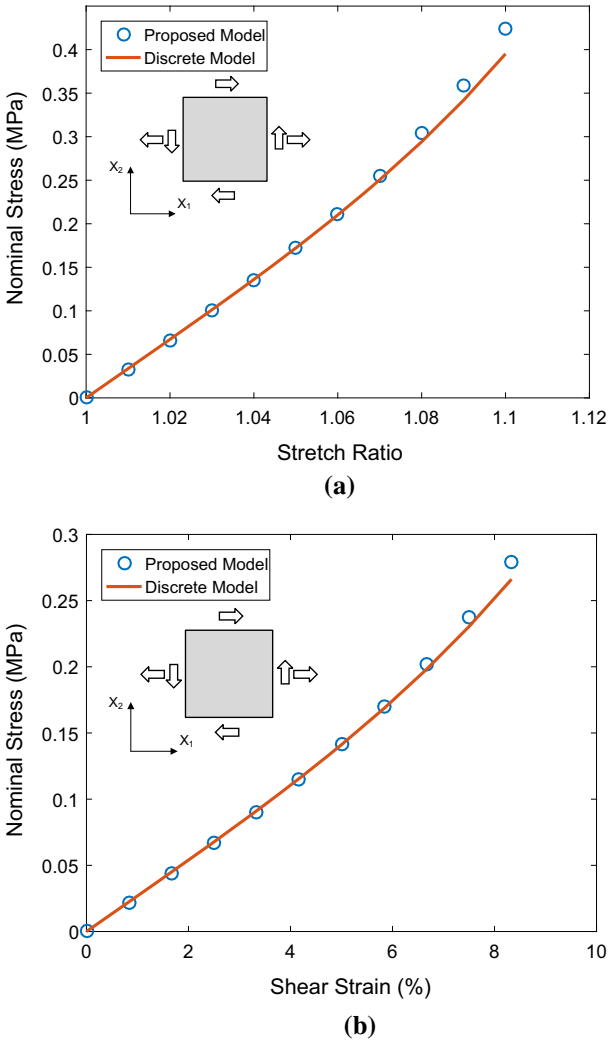

Fig. 8 Comparison of the combined normal and shear responses obtained from the proposed model and the discrete FE model. **a** Normal response. **b** Shear response

The initial lengths of the two fiber families are $L_{\mathrm{f}}^{(1)} = a_1$ and $L_{\mathrm{f}}^{(2)} = a_2$, respectively. The slack variable s is 1.0 which indicates that there is no slacking or pre-stretching in the fiber tows. Since the fiber orientations $\boldsymbol{A}_{\mathrm{f}}^{(1)}$ and $\boldsymbol{A}_{\mathrm{f}}^{(2)}$ are aligned with the X_1 and X_2 directions, respectively, the third term in the Cauchy stress [see Eq. (20)] contributes only to the normal components. The zero shear stress implies that the deformation gradient and the deformation tensors are given by

$$\boldsymbol{F} = \begin{pmatrix} \lambda_1 & 0 & 0 \\ 0 & \lambda_2 & 0 \\ 0 & 0 & \lambda_3 \end{pmatrix}, \tag{22}$$

$$\boldsymbol{C} = \boldsymbol{B} = \begin{pmatrix} \lambda_1^2 & 0 & 0 \\ 0 & \lambda_2^2 & 0 \\ 0 & 0 & \lambda_3^2 \end{pmatrix}. \tag{23}$$

The volume change ratio and the isochoric part of the deformation tensors are given by

$$J = \lambda_1 \lambda_2 \lambda_3, \tag{24}$$

$$\bar{\boldsymbol{B}} = \bar{\boldsymbol{C}} = J^{-2/3}\boldsymbol{C} = (\lambda_1\lambda_2\lambda_3)^{-2/3}\begin{pmatrix}\lambda_1^2 & 0 & 0\\ 0 & \lambda_2^2 & 0\\ 0 & 0 & \lambda_3^2\end{pmatrix}. \tag{25}$$

If only normal stresses are applied, the Cauchy stress tensor becomes

$$\boldsymbol{\sigma} = \begin{pmatrix}\sigma_{11} & 0 & 0\\ 0 & \sigma_{22} & 0\\ 0 & 0 & \sigma_{33}\end{pmatrix} \tag{26}$$

with

$$\sigma_{11} = (1-V_\mathrm{f})\left(\frac{\mu}{3J^{5/3}}\left(2\lambda_1^2-\lambda_2^2-\lambda_3^2\right)+K(J-1)\right)+\frac{E_\mathrm{f}V_\mathrm{f}a_1\lambda_1}{J(a_1+a_2)}\left(\frac{a_1\lambda_1+a_2\lambda_2}{a_1+a_2}-1\right), \tag{27}$$

$$\sigma_{22} = (1-V_\mathrm{f})\left(\frac{\mu}{3J^{5/3}}\left(2\lambda_2^2-\lambda_1^2-\lambda_3^2\right)+K(J-1)\right)+\frac{E_\mathrm{f}V_\mathrm{f}a_2\lambda_2}{J(a_1+a_2)}\left(\frac{a_1\lambda_1+a_2\lambda_2}{a_1+a_2}-1\right), \tag{28}$$

$$\sigma_{33} = (1-V_\mathrm{f})\left(\frac{\mu}{3J^{5/3}}\left(2\lambda_3^2-\lambda_1^2-\lambda_2^2\right)+K(J-1)\right). \tag{29}$$

For uniaxial tension, it is required that

$$\sigma_{22} = \sigma_{33} = 0. \tag{30}$$

Thus, the deformation responses, which are dictated by the stretch ratios, λ_1, λ_2, and λ_3, can be solved based on the prescribed stress σ_{11} using Eqs. (27)–(30).

To understand the effect of knitting architecture on the resulting performance, the uniaxial tensile responses are computed by varying the parameters a_1 and a_2, which are the characteristics of the knitting pattern, as shown in Fig. 1. Figure 9 shows the Cauchy stress (σ_{11}) versus stretch ratio (λ_1) response of the composites of various values of a_1 and a_2. The results are compared with the pure rubber response to illustrate the reinforcement effect. The pure rubber behavior is obtained by setting $E_\mathrm{f}V_\mathrm{f} = 0$. The material parameters used in this study are summarized in Table 2. Here, a large value of K indicates the incompressibility of the pure rubber, and E_f is an approximation of the Young's modulus of the Kevlar fiber.

It is obvious that by incorporating a small volume fraction of knitted fabrics ($V_\mathrm{f} = 2.0\%$), the reinforced composite shows a significant stiffer response compared with the results of pure rubber. It also shows that the

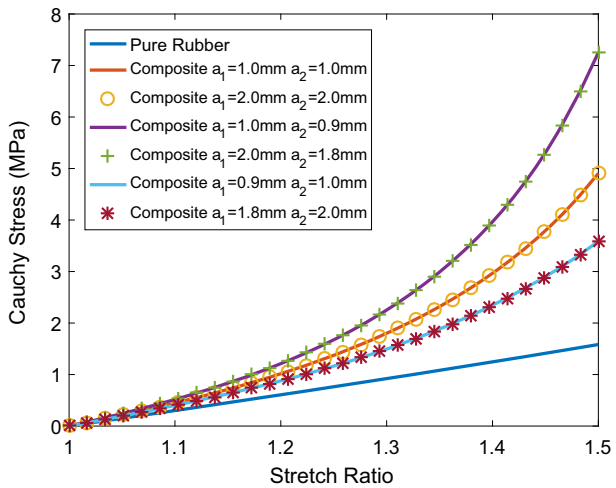

Fig. 9 Effects of the fabric construction on the composite response

Table 2 The rubber and fiber properties used in the parametric study of various architectures of knitted fabric reinforcement

μ (MPa)	K (MPa)	E_f (MPa)	V_f (%)
1.0	1.0×10^5	1.0×10^5	2.0

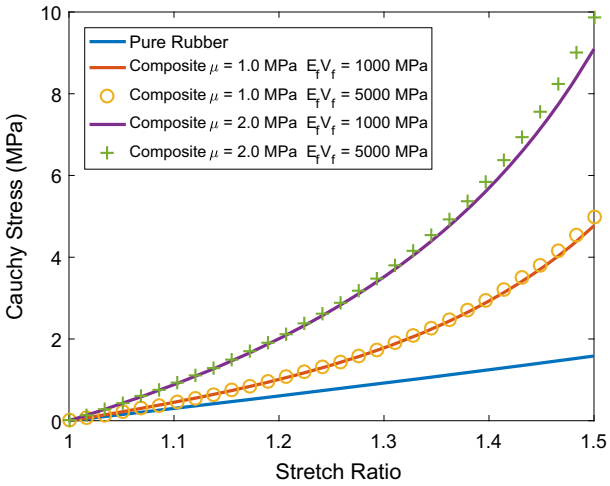

Fig. 10 Effects of the fiber properties on the composite response

reinforcement effect is determined by the ratio a_1/a_2. A higher ratio of a_1/a_2 provides more reinforcement effects along the X_1 direction. Since the fibers are orthogonally interlocked, this also implies that a lower ratio a_1/a_2 can stiffen the X_2 direction. Therefore, the knitting pattern can be tailored to achieve a specific reinforcement effect by designing the ratio of the parameters a_1 and a_2.

Another set of design parameters of the composite are the fiber and rubber properties and their volume fractions. Figure 10 shows the uniaxial stress–stretch responses of the composites of various fiber and rubber moduli. In this study, the fabric geometry is fixed by setting $a_1 = a_2 = 1$ mm. The rubber is assumed to be nearly incompressible with $K = 1.0 \times 10^5$ MPa. Based on the expressions of the strain energy function (Eq. 15) and the Cauchy stress (Eq. 20), the value of $E_\mathrm{f} V_\mathrm{f}$ can be treated as one material constant. Another important material property is the initial shear modulus of the rubber, which dictates the pure rubber deformation.

As shown in Fig. 10, the fiber property, $E_\mathrm{f} V_\mathrm{f}$, has little impact on the reinforcement effect. For this point, based on the numerical results, some care must be taken is that the independence on $E_\mathrm{f} V_\mathrm{f}$ happens when this value is much larger than the initial shear modulus. For a traditional strain energy function of an isotropic hyperelastic material, the initial bulk modulus usually acts as a constraint of the compressibility, which means that a larger initial bulk modulus will give a higher incompressibility of the material. In our model, the value of $E_\mathrm{f} V_\mathrm{f}$ acts similarly as the initial bulk modulus, but it provides the extensibility of the fiber, which means that a larger value of $E_\mathrm{f} V_\mathrm{f}$ provides a higher inextensibility of the fiber. The reinforcement of the knitted fabric comes from the inextensibility which acts as constraints of the deformation state. Another observation is that with the same fiber construction, the overall mechanical response is dominated by the mechanical property of the rubber.

To understand the effect of manufacturing processes on the resulting composite behavior, uniaxial tensile responses with various slack variables are studied. The fabric geometry and material properties are the same as those used in Sect. 3. As shown in Fig. 5, the composite shows a higher stiffness with a lower slack variable. This is because for a smaller slack variable, the fiber tows carry load earlier and contribute more reinforcement effects under the same deformation state. It is also evident that the composite shows a stiffer response when the fabric is pre-stretched, while the performance is reduced when the fabric is slacking at the initial state.

5 Conclusions

In this paper, an anisotropic hyperelastic model based on the strain energy density function has been developed to predict the deformation response of rubbers reinforced by knitted fabrics. The strain energy function incorporates both rubber nonlinear responses through the neo-Hookean model and the reinforcement effect due to fiber stretch. A slack variable is introduced to account for the effect of processing-induced fabric pre-stretch or fabric slack on the resulting composite behavior. It shows that due to the low extensibility of the fiber, the deformation of the rubber is constrained, resulting in an overall stiffening response of the composite. The proposed analytical model is validated through a discrete 3D FE analysis that models the fabric and rubber layers explicitly. The uniaxial tensile response of an orthogonally knitted composite is used as an example to demonstrate the predictive capability of the proposed model and illustrate the influence of the rubber and fabric

architecture on the resulting composite performance. It shows that the composite response is governed by the initial shear modulus of the rubber and the construction of the knitted fabric. The reinforcement effect depends on the ratio a_1/a_2 rather than the exact value of each parameter. A stiffer response is observed along the X_i direction with a higher ratio a_i/a_j, where a_i and a_j denote the fiber length along the X_i and X_j directions, respectively. Another material characteristic parameter, $E_\mathrm{f}V_\mathrm{f}$, controls the extensibility of the fiber. In addition, a pre-stretched fabric provides more reinforcement effects than a slack fabric.

The proposed model is based on the strain energy function approach; therefore, it yields a significant computational advantage since the computation can be carried out analytically. Since the model predicts the effect of constituent rubber property and fabric architecture on the resulting composite response, it can be employed to achieve virtual design of knitted-fabric-reinforced rubber composites with controlled macroscopic properties.

References

1. Huang, Z.M., Ramakrishna, S.: Micromechanical modeling approaches for the stiffness and strength of knitted fabric composites: a review and comparative study. Compos. Part A Appl. Sci. Manuf. **31**(5), 479–501 (2000)
2. Leong, K., Ramakrishna, S., Huang, Z., Bibo, G.: The potential of knitting for engineering compositesa review. Compos. Part A Appl. Sci. Manuf. **31**(3), 197–220 (2000)
3. ASTM D412-16, Standard Test Methods for Vulcanized Rubber and Thermoplastic ElastomersTension. ASTM International, West Conshohocken, PA (2016)
4. ASTM D380-94(2012), Standard Test Methods for Rubber Hose. ASTM International, West Conshohocken, PA (2012)
5. ASTM E143-13, Standard Test Method for Shear Modulus at Room Temperature. ASTM International, West Conshohocken, PA (2013)
6. Manach, P.Y.: Mechanical behavior of fabric-reinforced elastomer straight flexible hoses. Appl. Comput. Mech. **2**(1), 291–302 (2008)
7. Pidaparti, R.M., May, A.W.: A micromechanical analysis to predict the cord–rubber composite properties. Compos. Struct. **34**(4), 361–369 (1996)
8. Dinh, T., Rezaei, A., Daelemans, L., Mollaert, M., Van Hemelrijck, D., Van Paepegem, W.: A hybrid micro-meso-scale unit cell model for homogenization of the nonlinear orthotropic material behavior of coated fabrics used in tensioned membrane structures. Compos. Struct. **162**, 271–279 (2016)
9. Sun, W., Lin, F., Hu, X.: Computer-aided design and modeling of composite unit cells. Compos. Sci. Technol. **61**(2), 289–299 (2001)
10. Liu, D., Christe, D., Shakibajahromi, B., Knittel, C., Castaneda, N., Breen, D., Dion, G., Kontsos, A.: On the role of material architecture in the mechanical behavior of knitted textiles. Int. J. Solids Struct. **109**, 101–111 (2017)
11. Gough, V.: Stiffness of cord and rubber constructions. Rubber Chem. Technol. **41**(4), 988–1021 (1968)
12. Tangorra, G.: Fiber-reinforced, oriented rubber sheets. In: Proceedings of International Rubber Conference, Moscow, Russia, pp. 459–466 (1969)
13. Pidaparti, R.: Analysis of cord–rubber composite laminates under combined tension and torsion loading. Compos. Part B Eng. **28**(4), 433–438 (1997)
14. Rao, S., Daniel, I.M., Gdoutos, E.E.: Mechanical properties and failure behavior of cord/rubber composites. Appl. Compos. Mater. **11**(6), 353–375 (2004)
15. Qiu, G.Y., Pence, T.J.: Remarks on the behavior of simple directionally reinforced incompressible nonlinearly elastic solids. J. Elast. **49**, 1–30 (1997)
16. Holzapfel, G.A., Gasser, T.C., Ogden, R.W.: A new constitutive framework for arterial wall mechanics and a comparative study of material models. J. Elast. Phys. Sci. Solids **61**(1–3), 1–48 (2000)
17. Holzapfel, G.A., Gasser, T.C., Stadler, M.: A structural model for the viscoelastic behavior of arterial walls: continuum formulation and finite element analysis. Eur. J. Mech. A Solids **21**(3), 441–463 (2002)
18. Demirkoparan, H., Pence, T.J.: Swelling of an internally pressurized nonlinearly elastic tube with fiber reinforcing. Int. J. Solids Struct. **44**(11), 4009–4029 (2007)
19. Fereidoonnezhad, B., Naghdabadi, R., Arghavani, J.: A hyperelastic constitutive model for fiber-reinforced rubber-like materials. Int. J. Eng. Sci. **71**, 36–44 (2013)
20. Yang, H., Yao, X.F., Ke, Y.C., Ma, Y.J., Liu, Y.H.: Constitutive behaviors and mechanical characterizations of fabric reinforced rubber composites. Compos. Struct. **152**, 117–123 (2016)
21. Peng, X.Q., Guo, Z.Y., Moran, B.: An anisotropic hyperelastic constitutive model with fiber-matrix shear interaction for the human annulus fibrosus. J. Appl. Mech. **73**, 815–824 (2006)
22. Peng, X., Guo, G., Zhao, N.: An anisotropic hyperelastic constitutive model with shear interaction for cord rubber composites. Compos. Sci. Technol. **78**, 69–74 (2013)
23. Peng, X., Guo, Z., Du, T., Yu, W.R.: A simple anisotropic hyperelastic constitutive model for textile fabrics with application to forming simulation. Compos. Part B Eng. **52**, 275–281 (2013)
24. Nolan, D.R., Gower, A.L., Destrade, M., Ogden, R., McGarry, J.P.: A robust anisotropic hyperelastic formulation for the modelling of soft tissue. J. Mech. Behav. Biomed. Mater. **39**, 48–60 (2014)
25. Chebbi, E., Wali, M., Dammak, F.: An anisotropic hyperelastic constitutive model for short glass fiber-reinforced polyamide. Int. J. Eng. Sci. **106**, 262–272 (2016)